RSC Advances

PAPER



Cite this: *RSC Adv.*, 2021, **11**, 18776

# Effect of heteroatoms on the optical properties and enzymatic activity of N-doped carbon dots†

Ahyun Lee,‡ Sohee Yun,‡ Eun Soo Kang,‡ Jung Wan Kim, Jeong Ho Park and Jin-sil Choi*

Received 23rd April 2021
Accepted 17th May 2021

DOI: 10.1039/d1ra03175a

rsc.li/rsc-advances

Carbon dots (CDs) are attractive nanomaterials because of their facile synthesis, biocompatibility, superior physicochemical properties, and low cost of their precursors. Recent advances in CDs have particularly relied on the modulation of their properties by heteroatom doping (*e.g.*, nitrogen). Although nitrogen-doped CDs (**N-CDs**) have attracted considerable attention owing to their different properties compared to those of the original CDs, the effects of the heteroatom content and types of bonding on the properties of N-doped CDs remain underexplored. In this work, we prepared **N-CDs** with controlled nitrogen contents, and fully examined their optical properties, enzymatic activity, and toxicity. We demonstrate that (i) the type of carbon–heteroatom bonding (*i.e.*, carbon–oxygen and carbon–nitrogen bonds) can be altered by changing the ratio of carbon to heteroatom sources, and (ii) both the heteroatom content and the heteroatom-bonding character significantly influence the properties of the doped CDs. Notably, **N-CDs** exhibited higher quantum yields and peroxidase-like activities than the non-doped CDs. Furthermore, the negatively charged **N-CDs** exhibited negligible cytotoxicity. Such comprehensive investigations on the physicochemical properties of **N-CDs** are expected to guide the design of **N-CDs** for targeted applications.

## Introduction

Carbon dots (CDs) are an emerging class of nanomaterials that have attracted immense attention owing their easy accessibility through simple and low-cost synthetic processes, excellent optical properties, and biocompatibility.[1–4] Such new materials have great potential for a variety of applications, including cell labeling,[5–7] medical therapy,[8,9] sensing,[10] catalysis,[11,12] energy,[1,13–16] and energy storage.[14,15] In particular, one of the most attractive advantages of CDs is that their physicochemical properties can be tuned by controlling their size, surface state, and intrinsic electronic structures.[1–4] In this context, much effort has been devoted to the design and fabrication of heteroatom-doped CDs (*e.g.*, N-, B-, and S-doped CDs) and their application.[1,17,18] Among the heteroatom-doped CDs, nitrogen-doped CDs (**N-CDs**) are the most frequently utilized platform, because the nitrogen atoms are known to alter the edge states,[19,20] energy levels,[21–23] physicochemical properties,[6,13,17,19–22,24–31] and even catalytic activities[9,11,32–34] of the CDs. However, the effects of the heteroatom content and chemical bonding in CDs on their properties under subtle variation of the synthetic conditions are not fully understood.

In this work, we prepared a series of **N-CDs** by reacting citric acid with ethylenediamine at different ratios, and evaluated the optical properties and chemical composition of the resulting **N-CDs**. In addition, we also examined the enzyme-like activity of each **N-CD** in the series, and the influences of the N-doping type and N content on the catalytic activity. Finally, we also evaluated the toxicity of the **N-CDs** for assessing their potential applicability in biological studies.

## Experimental section

### Reagents

Citric acid (99.9%), ethylenediamine (>98%), quinine sulfate (98.0%), $H_2O_2$, 3,3′,5,5′-tetramethylbenzidine (TMB, 97%), and 3-(4,5-dimethylthiazol-2-yl)-2,5-diphenyltetrazolium bromide (MTT) assay kit were purchased from Sigma-Aldrich, and used as received.

### Synthesis of N-CDs

**N-CDs** were prepared by a hydrothermal method. In a typical synthesis, citric acid (10 μmol) and ethylenediamine (2.5–15 μmol) were dissolved in deionized water (15 mL), and the mixture was heated hydrothermally in a Teflon-equipped stainless steel autoclave at 200 °C. After 1 h, the mixture was cooled to room temperature, and the residue was purified by column chromatography (CombiFlash NextGen 100, Teledyne ISCO) to obtain a brown **N-CD** sample. The molar ratios of citric acid and ethylenediamine: **N-CD_1** = 1/1.5; **N-CD_2** = 1/1; **N-CD_3** = 1/0.5; **N-CD_4** = 1/0.33; **N-CD_5** = 1/0.25.

*Dept. of Chemical and Biological Engineering, Hanbat National University, 125 Dongseodaero Yuseonggu, Daejeon 34158, Republic of Korea. E-mail: jinsil.choi@hanbat.ac.kr*

† Electronic supplementary information (ESI) available: TEM images, size histogram, XRD, IR spectra, zeta-potential, and atomic percentage based on XPS spectra of **N-CDs** and none-doped CD. See DOI: 10.1039/d1ra03175a

‡ These authors contribute equally.

### Characterization

The morphology and lattice distance of **N-CDs** were investigated by transmission electron microscopy (TEM). A Tecnai $G^2$ F30 S-Twin system (FEI, Netherlands) and H-7650 system (Hitachi, Japan) installed in the Center for University-wide Research Facilities (CURF) at the Jeonbuk National University. X-ray diffraction (XRD) was performed on a Miniflex Benchtop X-ray diffractometer (Rigaku). The chemical functional groups and composition of the **N-CDs** were investigated by Fourier-transform infrared (FTIR) spectrometry (Nicolet 6700, Thermo, USA) and X-ray photoelectron spectrometry (XPS, K-Alpha+, Thermo Fisher Scientific, USA), respectively. Absorption and fluorescence spectra of the **N-CDs** were recorded on a UV-Vis spectrophotometer (Lambda 1050, PerkinElmer) and fluorescence spectrometer (QM-400, HORIBA), respectively. The fluorescence lifetime was measured using a fluorescence lifetime spectrometer (FL920, Edinburgh Instruments, United Kingdom).

### Quantum yield (QY) measurements

The relative quantum yield of the **N-CDs** was calculated as follows:

$$Q_s = Q_r \frac{m_s}{m_r} \frac{n_s}{n_r} \quad (1)$$

where $Q$ is the fluorescence QY, $m$ is the slope of the plot of the integrated fluorescence intensity against absorbance, and $n$ is the refractive index of the solvent. s and r represent the sample and reference, respectively. A solution of quinine sulfate in a 0.5 M $H_2SO_4$ aqueous solution was used as the reference (QY = 54.6%). The QY was determined through an average of three measurements under consistent experimental conditions.

### Enzyme-mimicking activities of N-CDs

The peroxidase-like activity was measured using TMB as the substrate. Specifically, a 1 M $H_2O_2$ solution, 100 μM TMB solution, and 500 μg $mL^{-1}$ **N-CD** suspension were added to a phosphate buffer (10 mM, pH 2), and the mixture was shaken thoroughly. The absorption of the sample at 652 nm was measured immediately using a multi-mode plate reader (SpectraMax M2e, Molecular Devices, LLC, USA). The Michaelis–Menten equation provides the relationship between the initial velocity, $V$, and the substrate concentration, [S].

$$V = \frac{[S]V_{max}}{[S] + K_m} \quad (2)$$

Here, $V_{max}$ is the maximum velocity of the enzymatic reaction, and $K_m$ is the Michaelis constant representing the concentration of the substrate at half the maximum velocity. The linear regression curve describing the relationship between $1/V$ and $1/[S]$, *viz.*, the Lineweaver–Burk plot, can be obtained by inverting the Michaelis–Menten equation to the following form:

$$\frac{1}{V} = \frac{K_m}{V_{max}} \frac{1}{[S]} + \frac{1}{V_{max}} \quad (3)$$

Upon plotting $1/V$ against $1/[S]$, the ordinate intercept of the curve represents the inverse of $V_{max}$ and the abscissa intercept represents $-1/K_m$. Thus, $K_m$ and $V_{max}$ were estimated.

### MTT assay

The biocompatibility and cytotoxicity of the **N-CDs** were evaluated using human lung cancer cells (A549) *via* the MTT assay.

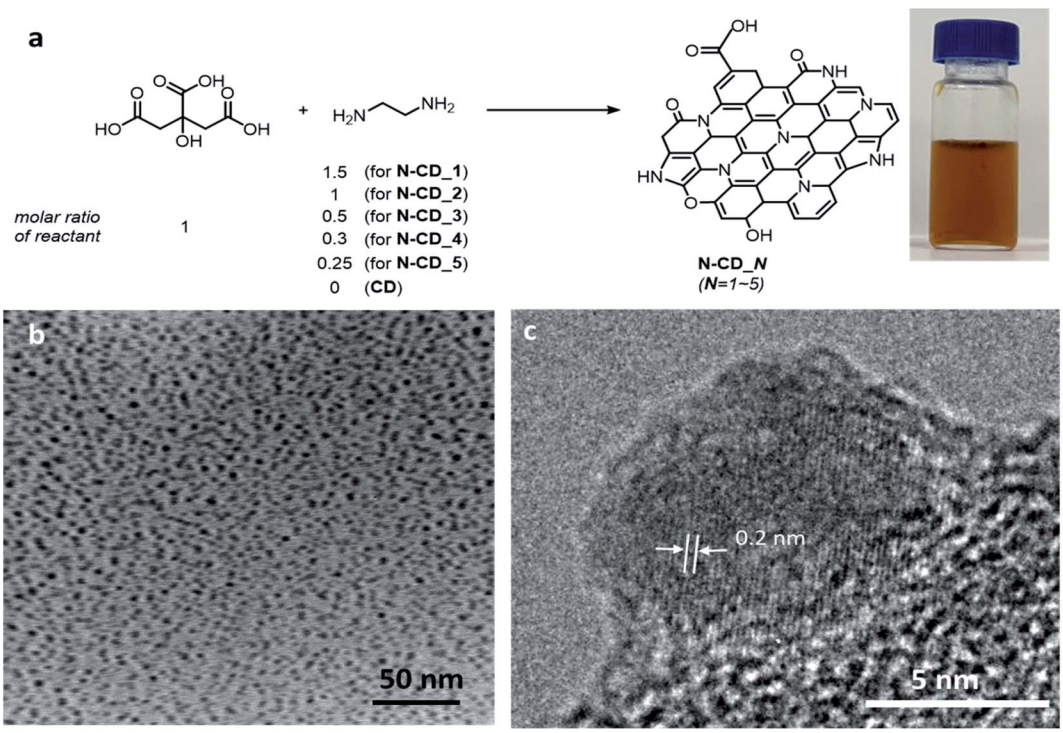


Fig. 1 (a) Schematics of the synthesis of N-doped carbon dots (**N-CDs**) and a photograph of the as-synthesized **N-CD** sample suspended in water. (b) Low- and (c) high-resolution TEM images of **N-CD_2**.

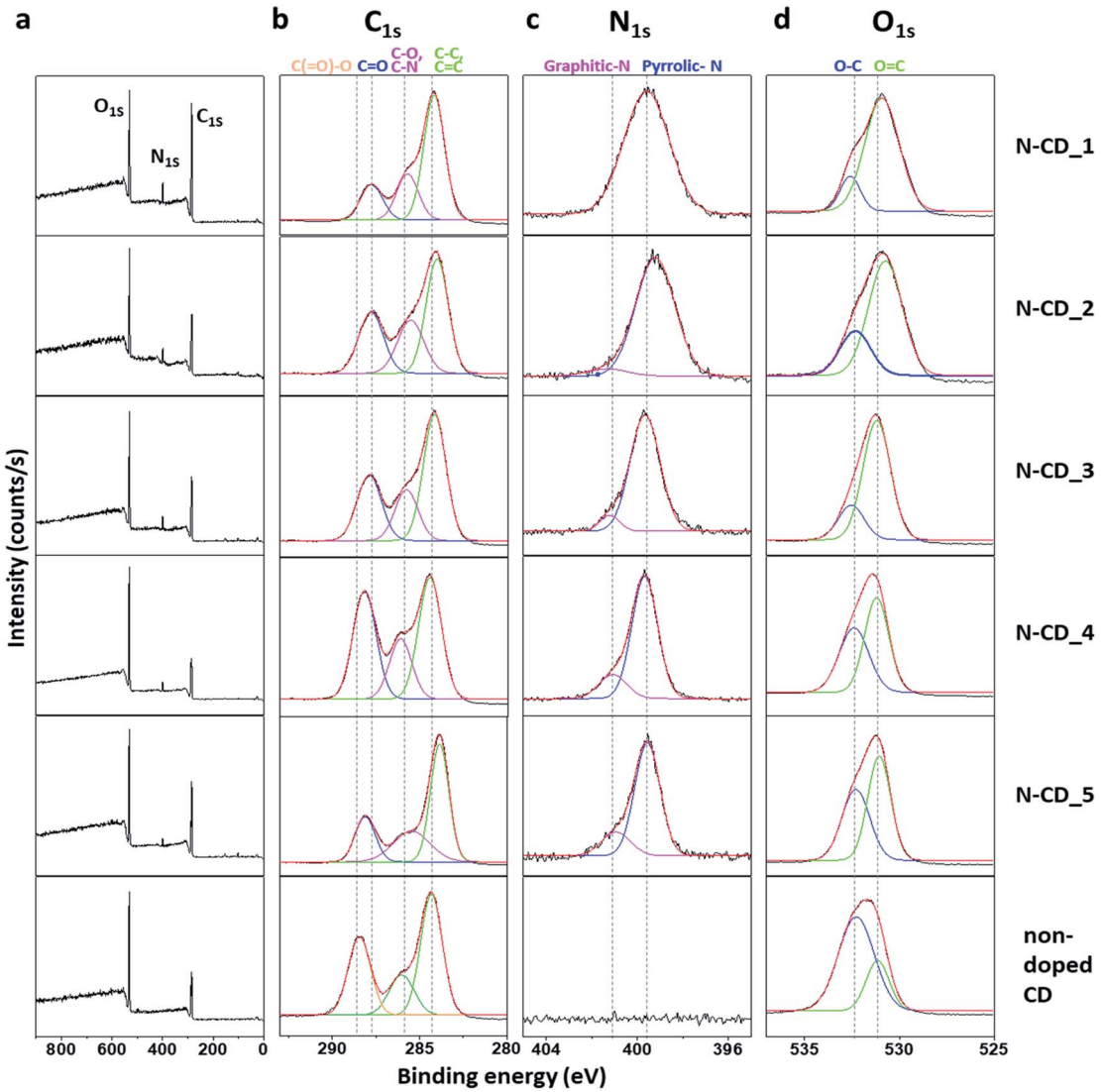


Fig. 2 (a) XPS survey scans and high-resolution (b) C 1s, (c) N 1s, and (d) O 1s spectra of **N-CDs** and non-doped **CD**.

A549 cells ($2 \times 10^5$ cells per well) were cultured overnight in a 96-well microtiter plate in 5% $CO_2$ atmosphere at 37 °C. The wells were charged with a cell medium containing **N-CDs** or **CDs** (15.6, 31.3, 62.5, 125.0, 250.0, and 500.0 μg $mL^{-1}$, respectively), and incubated for 24 h. Then, 10 μL of the MTT solution was added to each well (final concentration: 0.5 mg $mL^{-1}$). After incubation for 4 h, formazan, which is generated from the reduction of MTT by NAD(P)H-dependent oxidoreductase in living cells, was dissolved in the solubilization solution of the kit. The absorbance at 550 nm was obtained using a microplate reader (SpectraMax M2e, Molecular Devices, LLC, USA).

## Results and discussion

**N-CDs** were synthesized by a hydrothermal method (Fig. 1) by varying the ratio of citric acid (carbon source) to ethylenediamine (nitrogen source) from 1 : 1.5 (**N-CD_1**) to 1 : 1 (**N-CD_2**), 1 : 0.5 (**N-CD_3**), 1 : 0.3 (**N-CD_4**), and 1 : 0.25 (**N-CD_5**). The so-obtained brown **N-CDs** dispersed well in water (Fig. 1a). The TEM images in Fig. 1b and c reveal that **N-CD_3** has a spherical morphology with a diameter of 5.9 ± 1.3 nm; further, it is found to be partial crystalline with a lattice distance of 0.2 nm, which matches with the (100) plane of graphite.[20,21] However, a partial amorphous region is also observed at the edge site. The sizes of **N-CD_1, 2, 4, 5,** and non-doped **CD** samples were determined to be 13.7 ± 4.1, 4.9 ± 0.9, 7.8 ± 2.7, 4.5 ± 1.1, and 6.5 ± 1.8 nm, respectively (Fig. S1 and S2†). XRD patterns of the **N-CD** series display a broad diffraction peak, confirming their amorphous character (Fig. S3†).

Comparison of the FT-IR spectra of **N-CDs** with those of citric acid and ethylenediamine indicated the appearance of new peaks at 1673 and 1549–1410 $cm^{-1}$, corresponding to the C=C stretching of conjugated alkenes and C–N stretching of aromatic amines, respectively (Fig. S4†). In addition, new peaks corresponding to N–O and C=N appeared at 1546 and 1783 $cm^{-1}$, respectively, in the spectra of the **N-CD** series. The obtained **N-CDs** have a net negative charge owing to the

presence of abundant –COOH groups derived from citric acid (Fig. S5†). The chemical composition of the **N-CD** series was further examined by XPS (Fig. 2). The XPS survey profiles of all the **N-CD** samples (Fig. 2a and S6†) exhibit $C_{1s}$, $N_{1s}$, and $O_{1s}$ signals. However, the peak intensity ratios are significantly different between the samples. Interestingly, **N-CD_2** and **N-CD_4** show the highest peak intensities of $N_{1s}$ and $O_{1s}$, respectively, while **N-CD_4** shows the lowest peak intensity of $C_{1s}$. To gain more information about the chemical bonding of the different atoms, high-resolution $C_{1s}$, $N_{1s}$, and $O_{1s}$ spectra of the samples were analyzed by spectral peak fitting based on the reported binding energies of the chemical bonds, as demonstrated in Fig. 2b–d, respectively. First, the $C_{1s}$ spectra of all the **N-CD** samples show a strong peak at 284 eV, corresponding to C–C and C=C bonds, along with a peak at 285.5 eV for the C–N bond, indicating N doping, and a peak at 288.2 eV for C=O. The peaks of $C_{C-C}$ and $C_{C=C}$ represent the C atoms of the carbogenic $sp^2$ core, while the peaks of carbon–heteroatom bonds (*i.e.*, C–N and C=O) indicate the functional groups at the edge region of the **N-CDs**. Among the **N-CD** samples, **N-CD_2**, **3**, and **4** exhibit a relatively high intensity ratio of carbon–heteroatom bonds over carbon–carbon bonds. Non-doped **CDs** show strong peaks at 288.8 eV (C=O and C–O) and 284 eV (C–C and C=C). Meanwhile, the $N_{1s}$ spectra (Fig. 2c) of all the **N-CDs** show a strong peak of $N_{pyrrole}$ (399.5 eV), which is located at the edge sites of the carbogenic domain. The peak of $N_{graphite}$ (401 eV) located within the $sp^2$-carbon domain appeared in the spectra of **N-CD_2**, **3**, **4**, and **5**.[35–37] Furthermore, the $O_{1s}$ spectra consist of two peaks corresponding to C–O and C=O bonds (532.6 and 531.1 eV, respectively), with the $O_{C=O}$ peak being predominant in all **N-CD** samples, owing to the polymerization of the material through amide bond formation.[38,39] On the other hand, $O_{C-O}$ peak is dominant in the spectrum of the non-doped **CD**.

Next, the optical properties of the **N-CDs** were investigated (Fig. 3). A new absorption band at 340 nm (C=O, n → π*) and a shoulder band at 240 nm (–C=C–, π → π*) appeared in all the UV-Vis spectra of **N-CD** samples as compared to that of the non-doped **CD**. The absorption band at 340 nm is assigned to the n–π* transition arising from the edge transition of the **N-CD** samples, while the shoulder band at 240 nm originates from the π–π* transition at the $sp^2$ carbogenic domain. Non-doped **CDs** showed negligible absorption band at 340 nm owing to the small quantity of C=O bonds in the particle. The photoluminescence (PL) spectrum of each **N-CD** sample ($\lambda_{ex}$ = 350 nm) was found to be distinct. On one hand, **N-CD_1** and **N-CD_2** showed two emission bands. The PL peaks of **N-CD_1** appeared at 450 nm and 517 nm, while those of **N-CD_2** appeared at 450 nm and 500 nm. On the other hand, **N-CD_3**, **4**, and **5** exhibited only one emission peak. **N-CD_3** and **N-CD_4** showed a peak at 450 nm, which is the first emission peak observed for **N-CD_1**, **N-CD_2**, and non-doped **CD**, while **N-CD_5** showed a red-shifted emission band at 464 nm. It is known that $N_{graphite}$ can induce red-shifted emission, whereas $N_{pyrrole}$ does not affect the bandgap of the π-conjugated carbogenic domains.[20,23,26] However, in our study, red-shifted emissions were observed with **N-CD_1**, **2**, and **5**, which mostly

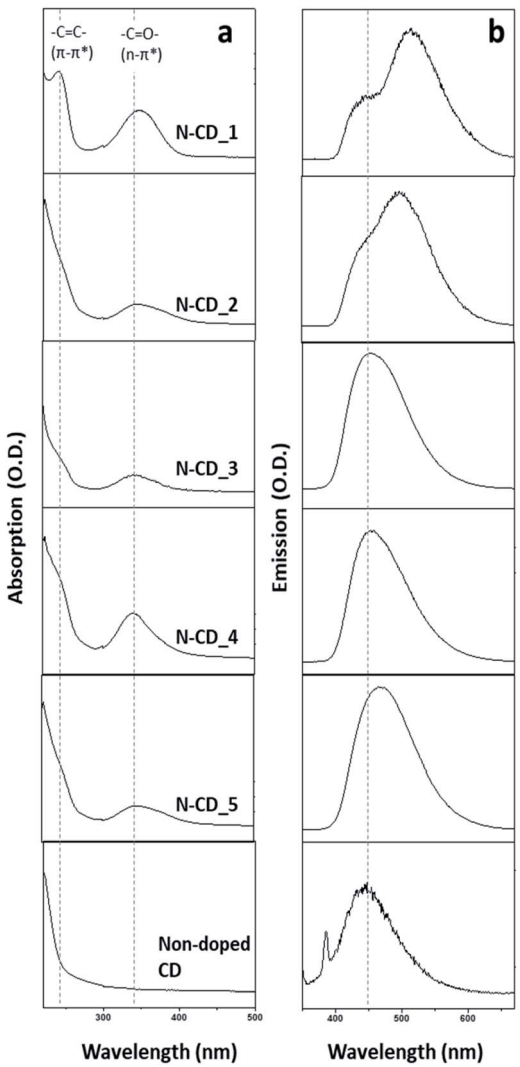


Fig. 3 (a) Absorption and (b) emission spectra of **N-CD** samples and non-doped **CD**.

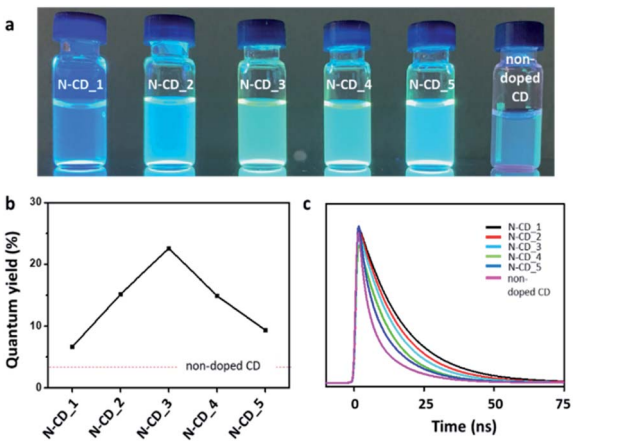


Fig. 4 (a) Photograph of the suspensions of the **N-CD** samples and non-doped **CD** placed on top of a UV lamp (365 nm). (b) Quantum yield and (c) fluorescence lifetime of the **N-CDs** and non-doped **CD** ($\lambda_{ex}$ = 350 nm, $\lambda_{em}$ = 450 nm).

contain $N_{pyrrole}$ along with a small quantity of other functional groups ($N_{graphite}$). Considering that increasing the number of edge functional groups in **N-CDs** results in a decrease in the size of the π-conjugated carbogenic domains,[18] it can be inferred that **N-CD_3** and **4**, which have a relatively low C content, emit high-energy light owing to the small size of their carbogenic domain. The red-shifted emissions of **N-CD_1**, **2**, and **5** could be attributed to the expanded size of the π-conjugated carbogenic domains with a relatively less amount of the dopant.[18,24]

Further, all the **N-CDs** displayed blue fluorescence under the excitation of 340 nm UV light, as shown in Fig. 4a. However, their emission brightness at the same concentration varied depending on the sample. To investigate the effect of the N dopant on the optical properties of **N-CDs**, we measured the QY of each **N-CD** ($\lambda_{ex} = 350$ nm; $\lambda_{em} = 450$ nm; Fig. 4b). The QYs of the five **N-CD** samples (**N-CD_1** to **5**) were estimated to be 6.6, 15.1, 22.6, 14.9, and 9.3%, respectively; they are higher than that of the non-doped **CD** (QY: ~3%). To gain further insights into the exciton recombination dynamics, the time-resolved PL decay was recorded ($\lambda_{ex} = 350$ nm; $\lambda_{em} = 450$ nm; Fig. 4c). All the **N-CDs** showed a dual exponential PL decay, and the PL lifetimes ($\tau_1/\tau_2$) of **N-CD_1** to **5** were determined to be 7.4/29.8, 6.2/24.9, 5.7/23.0, 5.0/20.0, and 4.8/19.5 ns, respectively. Evidently, the PL lifetimes of the **N-CD** samples are longer than that of the non-doped **CD** ($\tau_1 = 4.2$ ns and $\tau_2 = 17.05$ ns) because the surface passivation of the **CD** by N-doping can decrease the nonradiative recombination and self-trapping of excitons.[3,18,40] The QY of the **N-CDs** decreased with a decrease in the N content (**N-CD_3** to **5**), and the lifetime was shortened. Interestingly, the QYs of **N-CD_1** and **2** were found to be lower than that of **N-CD_3**, although their PL lifetimes were longer. This phenomenon may be attributed to the large quantity of N dopant, which can generate long-lived defect states at the surface of **N-CDs**.[41–44] Thus, the N-dopant content in the **N-CDs** is a critical factor that affects their optical properties, and according to our evaluation, **N-CD_3** is the most effective candidate as an optical probe.

Next, we explored the application of **N-CDs** as a nanozyme platform. A nanozyme is a material that can catalyze enzymatic reactions; it exhibits similar enzymatic kinetics and mechanism to those of natural enzymes.[8] As **N-CDs** have been reported to mimic the peroxidase enzyme,[11] we evaluated the peroxidase-like activities of our **N-CDs** by monitoring the oxidation of TMB with $H_2O_2$ in their presence at pH 2 (Fig. 5a). The addition of **N-CDs** to a solution of $H_2O_2$ and TMB resulted in a color change from pale green to blue, indicating the oxidation of TMB (Fig. 5b). The absorbance of the TMB solution at 652 nm originates from oxidized TMB, whose quantity increases gradually as a result of the enzymatic reaction in the presence of the **N-CDs** as well as the non-doped **CD**. The measured absorbance eventually saturated after a sufficient reaction time, as in the case of a natural enzymatic reaction (Fig. 5c). Remarkably, the **N-CDs** showed a faster rate of TMB oxidation than the non-doped **CD**. To acquire the kinetic parameters related to the activity of **N-CDs**, the steady-state kinetics of the reaction was studied by measuring the absorbance at 652 nm at different $H_2O_2$ concentrations. The maximum initial velocity ($V_{max}$) and Michaelis constant ($K_m$) of the reaction in the presence of **N-CDs** were calculated based on the Lineweaver–Burk equation (Fig. 5d). All the **N-CDs** provided higher $V_{max}$ values than the non-doped **CD**, and the $V_{max}$ of the **N-CDs** increased in the order

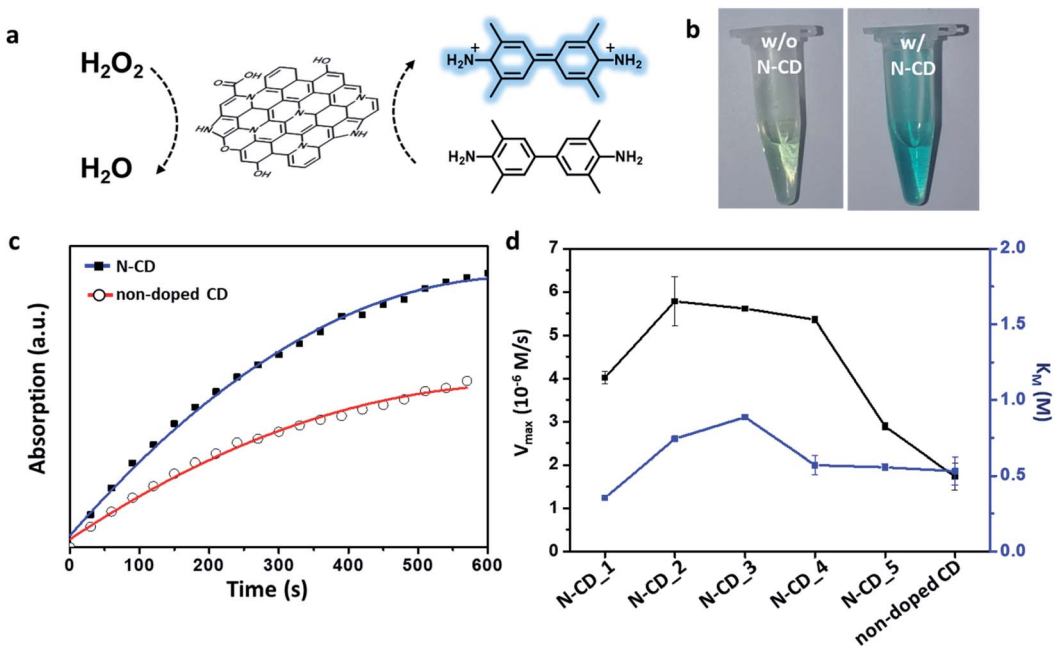


Fig. 5 (a) Schematic illustration of the peroxidase mimetic activity of **N-CDs** and (b) images of TMB/$H_2O_2$ solutions with and without **N-CDs**. (c) Kinetic curves of **N-CD** and non-doped **CD** for monitoring the catalytic oxidation of TMB (10 mM phosphate buffer, pH 2.0) with 1 M $H_2O_2$ in the presence of the **N-CD** or non-doped **CD**. (d) Comparison of the $V_{max}$ and $K_m$ values of **N-CDs** and non-doped **CD**; these were calculated from the Lineweaver–Burk plot.

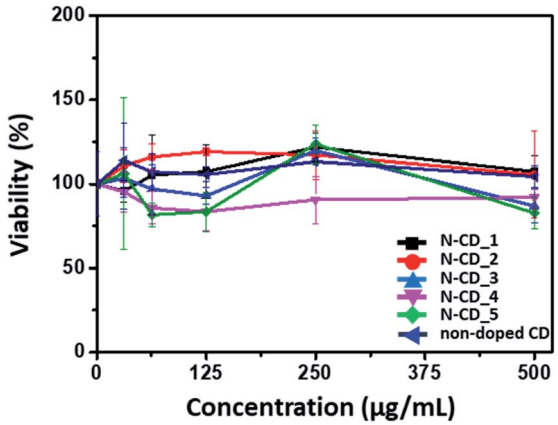


Fig. 6 Viability test of the N-CD samples and non-doped CD. Viability of A549 cells was examined using the MTT assay, in which A549 cells were treated with a cell medium containing the N-CD or non-doped CD for 24 h.

of **N-CD_5**, **1**, **4**, **3**, and **2**. In particular, **N-CD_2**, **3**, and **4** showed *ca.* 2.5–3 times higher $V_{max}$ values than that of the non-doped **CD**. Notably, the initial reaction velocities in the presence of **N-CD_1** and **5** were relatively lower than those in the presence of other **N-CDs**. The $K_m$ value, which represents the affinity between a substrate and enzyme, was found to be similar, regardless of the N-doping characteristic of the **N-CD** sample. According to our observations, the bond character of the heteroatom in the **N-CDs** affects $V_{max}$ rather than $K_m$. The C=O groups, which are present in abundance in **N-CDs**, are reported to act as the catalytic sites.[34,45] Thus, most of the **N-CDs** exhibited higher $V_{max}$ than that of non-doped **CD**, which is rich C–O groups than in C=O groups. In addition, the graphitic N atoms help adsorb molecular oxygen to generate radical oxygen species on nearby carbon atoms.[9,11,32,46] Consequently, an **N-CD** sample with graphitic N and abundant C=O groups showed a relatively high peroxidase-like activity. On the other hand, because the pyrrole moiety does not have extra electrons that can interact with $H_2O_2$, **N-CD_1** and **N-CD_5**, which mostly contain $N_{pyrrole}$, exhibited low catalytic activities.[26] Although **N-CD_5** has graphitic N atoms, its $N_{graphite}$ content is not sufficient to significantly improve the enzymatic activity, considering the N-doping degree shown in Fig. S6.† Therefore, the chemical composition of heteroatom-containing functional groups in **N-CDs** is an important factor for optimizing their enzymatic properties.

Finally, we investigated the toxicity of the **N-CDs** to assess if the **N-CD** platform can be applied in biological studies by evaluating the viability of human lung cancer cells, A549 cells, in the presence of the **N-CDs** and non-doped **CD**. As shown in Fig. 6, none of the **N-CDs** exhibited significant toxicity to the cells up to a concentration of 500 μg $mL^{-1}$. In fact, while the doping of N in the **N-CDs** could induce a local positive charge, the negatively charged **N-CDs** obtained in this study, owing to the usage of citric acid as the carbon source, may not disturb or interact significantly with the cell membrane, thus inducing negligible cellular toxicity.

## Conclusions

The characteristics of **N-CDs** suitable for their optical applications or for use as nanozymes were demonstrated by rationalizing the relationship between the dopant content (*e.g.*, the amount of doped N and types of chemical bonding) and physicochemical properties. The negligible cellular toxicity of the obtained **N-CDs** was also demonstrated, revealing their suitability for biological applications. As the doping content and bonding character are altered at the synthesis stage, an understanding of the correlation between the synthetic condition and heteroatom doping in **N-CDs** would be useful for producing **N-CDs** with desired features. Comprehensive investigations on the physicochemical properties of the **N-CDs** may provide further guidelines for the rational design of optimally performing **N-CDs**.

## Conflicts of interest

There are no conflicts to declare.

## Acknowledgements

This work was supported by the newly appointed professor research fund of Hanbat National University in 2018 and the National Research Foundation of Korea (NRF) grant funded by the Korea government (MSIT) (2020R1C1C1011863 and 2020R1A5A8017671).

## References

1 Y. Choi, Y. Choi, O.-H. Kwon and B.-S. Kim, *Chem.–Asian J.*, 2018, **13**, 586–598.
2 B. Yao, H. Huang, Y. Liu and Z. Kang, *Trends Chem.*, 2019, **1**, 235–246.
3 M. L. Liu, B. B. Chen, C. M. Li and C. Z. Huang, *Green Chem.*, 2019, **21**, 449–471.
4 R. Das, R. Bandyopadhyay and P. Pramanik, *Mater. Today Chem.*, 2018, **8**, 96–109.
5 R. Atchudan, T. N. J. I. Edison, M. G. Sethuraman and Y. R. Lee, *Appl. Surf. Sci.*, 2016, **384**, 432–441.
6 Y. He, L. Liang, Q. Liu, J. Guo, D. Liang and H. Liu, *RSC Adv.*, 2017, **7**, 56087–56092.
7 X. Wang, D. Wang, Y. Guo, C. Yang, A. Iqbal, W. Liu, W. Qin, D. Yan and H. Guo, *Dalton Trans.*, 2015, **44**, 5547–5554.
8 K. Fan, J. Xi, L. Fan, P. Wang, C. Zhu, Y. Tang, X. Xu, M. Liang, B. Jiang, X. Yan and L. Gao, *Nat. Commun.*, 2018, **9**, 1440.
9 Y. Zhang, Y. Jin, H. Cui, X. Yan and K. Fan, *RSC Adv.*, 2020, **10**, 10–20.
10 J.-X. Wu and B. Yan, *Dalton Trans.*, 2017, **4745**, 7098–7105.
11 Y. Hu, X. J. Gao, Y. Zhu, F. Muhammad, S. Tan, W. Cao, S. Lin, Z. Jin, X. Gao and H. Wei, *Chem. Mater.*, 2018, **30**, 6431–6439.
12 M. J. Lázaro, S. Ascaso, S. Pérez-Rodríguez, J. C. Calderón, M. E. Gálvez, M. Jesús Nieto, R. Moliner, A. Boyano,

D. Sebastián, C. Alegre, L. Calvillo and V. Celorrio, *C. R. Chim.*, 2015, **18**, 1229–1241.
13 X. T. Feng, F. Zhang, Y. L. Wang, Y. Zhang, Y. Z. Yang and X. G. Liu, *Appl. Phys. Lett.*, 2015, **107**, 213102.
14 V. C. Hoang, K. Dave and V. G. Gomes, *Nano Energy*, 2019, **66**, 104093.
15 C. Hu, M. Li, J. Qiu and Y.-P. Sun, *Chem. Soc. Rev.*, 2019, **48**, 2315–2337.
16 H. Ming, Z. Ma, Y. Liu, K. Pan, H. Yu, F. Wang and Z. Kang, *Dalton Trans.*, 2012, **41**, 9526–9531.
17 J. Manioudakis, F. Victoria, C. A. Thompson, L. Brown, M. Movsum, R. Lucifero and R. Naccache, *J. Mater. Chem. C*, 2019, **7**, 853–862.
18 X. Kou, S. Jiang, S.-J. Park and L.-Y. Meng, *Dalton Trans.*, 2020, **49**, 6915–6938.
19 L. Li and T. Dong, *J. Mater. Chem. C*, 2018, **6**, 7944–7970.
20 X. Miao, D. Qu, D. Yang, B. Nie, Y. Zhao, H. Fan and Z. Sun, *Adv. Mater.*, 2018, **30**, 1704740.
21 D. Mombrú, M. Romero, R. Faccio and Á. W. Mombrú, *Phys. E*, 2019, **113**, 130–136.
22 J. Schneider, C. J. Reckmeier, Y. Xiong, M. von Seckendorff, A. S. Susha, P. Kasák and A. L. Rogach, *J. Phys. Chem. C*, 2017, **121**, 2014–2022.
23 K. Holá, M. Sudolská, S. Kalytchuk, D. Nachtigallová, A. L. Rogach, M. Otyepka and R. Zbořil, *ACS Nano*, 2017, **11**, 12402–12410.
24 S. Barman and M. Sadhukhan, *J. Mater. Chem.*, 2012, **22**, 21832.
25 H. Wang, P. Gao, Y. Wang, J. Guo, K.-Q. Zhang, D. Du, X. Dai and G. Zou, *APL Mater.*, 2015, **3**, 086102.
26 S. Sarkar, M. Sudolská, M. Dubecký, C. J. Reckmeier, A. L. Rogach, R. Zbořil and M. Otyepka, *J. Phys. Chem. C*, 2016, **120**, 1303–1308.
27 Y. R. Park, H. Y. Jeong, Y. S. Seo, W. K. Choi and Y. J. Hong, *Sci. Rep.*, 2017, **7**, 46422.
28 R. Shi, Z. Li, H. Yu, L. Shang, C. Zhou, G. I. N. Waterhouse, L.-Z. Wu and T. Zhang, *ChemSusChem*, 2017, **10**, 4650–4656.
29 A. A. Kokorina, A. A. Bakal, D. V. Shpuntova, A. Yu. Kostritskiy, N. V. Beloglazova, S. De Saeger, G. B. Sukhorukov, A. V. Sapelkin and I. Y. Goryacheva, *Sci. Rep.*, 2019, **9**, 14665.
30 M. Xu, S. Xu, Z. Yang, M. Shu, G. He, D. Huang, L. Zhang, L. Li, D. Cui and Y. Zhang, *Nanoscale*, 2015, **7**, 15915–15923.
31 S. Bhattacharyya, F. Ehrat, P. Urban, R. Teves, R. Wyrwich, M. Döblinger, J. Feldmann, A. S. Urban and J. K. Stolarczyk, *Nat. Commun.*, 2017, **8**, 1401.
32 Z. Lou, S. Zhao, Q. Wang and H. Wei, *Anal. Chem.*, 2019, **91**, 15267–15274.
33 Q. Chen, S. Li, Y. Liu, X. Zhang, Y. Tang, H. Chai and Y. Huang, *Sens. Actuators, B*, 2020, **305**, 127511.
34 H. Sun, A. Zhao, N. Gao, K. Li, J. Ren and X. Qu, *Angew. Chem., Int. Ed.*, 2015, **54**, 7176–7180.
35 We believe nitrogen atoms distribute homogenously in our **N-CD** system based on the ref. 36 and 37 describing the homogeneous distribution of nitrogen atoms in the whole nitrogen-doped carbon-based materials regardless of types of functional groups based on STEM-EDX mapping studies.
36 J.-H. Wee, C. H. Kim, H.-S. Lee, G. B. Choi, D.-W. Kim, C.-M. Yang and Y. A. Kim, *Sci. Rep.*, 2019, **9**, 20170.
37 E. Haque, M. M. Islam, E. Pourazadi, M. Hassan, S. N. Faisal, A. K. Roy, K. Konstantinov, A. T. Harris, A. I. Minett and V. G. Gomes, *RSC Adv.*, 2015, **5**, 30679–30686.
38 P. Duan, B. Zhi, L. Coburn, C. L. Haynes and K. Schmidt-Rohr, *Magn. Reson. Chem.*, 2020, **58**, 1130–11389.
39 R. C. So, J. E. Sanggo, L. Jin, J. M. A. Diaz, R. A. Guerrero and J. He, *ACS Omega*, 2017, **2**, 5196–5208.
40 H. Zheng, P. Zheng, L. Zheng, Y. Jiang, Z. Wu, F. Wu, L. Shao, Y. Liu and Y. Zhang, *J. Phys. Chem. C*, 2018, **122**, 29613–29619.
41 C.-Q. Wang, J.-X. Xia, M. U. Ali, M. Liu, W. Lu and H. Meng, *Mater. Sci. Semicond. Process.*, 2019, **92**, 96–102.
42 N. T. Hien, T. T. K. Chi, N. D. Vinh, H. T. Van, L. D. Thanh, P. V. Do, V. P. Tuyen and N. X. Ca, *J. Lumin.*, 2020, **217**, 116822.
43 B. Xu, T. Zhang, X. Lin, H. Yang, X. Jin, Z. Huang, Z. Zhang, D. Li and Q. Li, *Opt. Mater. Express*, 2020, **10**, 1232–1240.
44 M. S. Mehata and T. C. Wang, *Dalton Trans.*, 2019, **4845**, 7619–7631.
45 S.-C. Wei, Y.-W. Lin and H.-T. Chang, *J. Food Drug Anal.*, 2020, **28**, 559–575.
46 H. Zhang, S. Hwang, M. Wang, Z. Feng, S. Karakalos, L. Luo, Z. Qiao, X. Xie, C. Wang, D. Su, Y. Shao and G. Wu, *J. Am. Chem. Soc.*, 2017, **139**, 14143–14149.